

## Investigation of the parallel gradation method based on the response of track-bed materials under cyclic loadings

Shuai Qi, Yu Jun Cui, Jean Claude Dupla, Ren-Peng Chen, Han-Lin Wang,

Yu Su, Francisco Lamas-Lopez, Jean Canou

#### ► To cite this version:

Shuai Qi, Yu Jun Cui, Jean Claude Dupla, Ren-Peng Chen, Han-Lin Wang, et al.. Investigation of the parallel gradation method based on the response of track-bed materials under cyclic loadings. Transportation Geotechnics, 2020, 24, pp.100360. 10.1016/j.trgeo.2020.100360. hal-03045872

### HAL Id: hal-03045872 https://enpc.hal.science/hal-03045872

Submitted on 28 May 2021  $\,$ 

**HAL** is a multi-disciplinary open access archive for the deposit and dissemination of scientific research documents, whether they are published or not. The documents may come from teaching and research institutions in France or abroad, or from public or private research centers. L'archive ouverte pluridisciplinaire **HAL**, est destinée au dépôt et à la diffusion de documents scientifiques de niveau recherche, publiés ou non, émanant des établissements d'enseignement et de recherche français ou étrangers, des laboratoires publics ou privés.

1	Investigation of the parallel gradation method based on the response of
2	track-bed materials under cyclic loadings
3	
4	Shuai Qi <sup>1, 2</sup> , Yu-Jun Cui <sup>2</sup> , Jean-Claude Dupla <sup>2</sup> , Ren-Peng Chen <sup>1</sup> , Han-Lin Wang <sup>3</sup> , Yu
5	Su <sup>2</sup> , Francisco Lamas-Lopez <sup>2</sup> , Jean Canou <sup>2</sup>
6	
7	1: Zhejiang University, China
8	2: Laboratoire Navier/CERMES, Ecole des Ponts ParisTech (ENPC), France
9	3: Department of Civil and Environmental Engineering, The Hong Kong Polytechnic
10	University, Hung Hom, Kowloon, Hong Kong, China
11	
12	
13	
14	
15	
16	
17	
18	Corresponding author:
10	
19	Mr. Shuai Qi
20	Department of Civil Engineering
21	Zhejiang University, Hangzhou, China
22	E-mail: <u>qishuailw@163.com</u>

#### 23 Abstract

Ballast/fines mixture is often found in railway substructure and the overall behaviour 24 25 of tracks is strongly dependent on the mechanical behaviour of this mixture. Since directly testing such mixture with large grains is limited with common laboratory 26 equipment, the consideration of a model material at smaller size is advisable. Parallel 27 gradation method is widely used for this purpose. This study assesses the validity of 28 this method in the case of ballast/fines mixture. Large-scale cyclic triaxial tests were 29 carried out on the ballast/fines mixture at six volumetric coarse grain contents. The 30 31 results obtained were analysed, together with those obtained previously from small-scale triaxial tests on a microballast/fines mixture whose microballast grain size 32 distribution was determined by applying the parallel gradation method. The cyclic 33 34 parameters (permanent strain and resilient modulus) were obtained for the two types of mixture. Results show that for all mixtures two distinct soil fabrics can be 35 identified according to the variations of permanent strain and resilient modulus with 36 the volumetric content of coarse grains  $f_v$ : a fine-fine contact structure for  $f_v \le 20\%$ 37 and a grain-grain contact structure for  $f_v \ge 35\%$ . In the case of fine-fine contact 38 39 structure, the permanent strains and resilient modulus values of the ballast specimens are consistent with those of the microballast specimens, evidencing the validity of the 40 parallel gradation method. In the case of grain-grain contact structure, the permanent 41 strains and resilient modulus values are found to coincide globally at the two scales, 42 also justifying the validity of the parallel gradation method, the slight differences 43 between the two scales being attributed to the irregular grain sliding and the 44

- 45 distribution of the fines soils.
- 46
- 47 Keywords: interlayer soil; cyclic triaxial tests; permanent deformation; resilient
- 48 modulus; parallel gradation method

#### 49 **1. Introduction**

Ballast/fines mixture is often found in railway substructure [10,17]. For instance, in 50 51 the French conventional railway lines (representing 94% of the total railway network), there is an interlayer which was formed by interpenetration of ballast and subgrade 52 53 soils under the effect of train circulation [10]. During the renewable program for conventional lines, this layer was maintained since the dry density of the interlayer 54 was as high as 2.4 Mg/m<sup>3</sup> and thus a favourable mechanical behaviour was expected 55 [7]. According to the in-situ investigation, the soil fabric of the interlayer is found to 56 57 be greatly dependent on the content of ballast grains [37,38]: the ballast grains are in contact with each other for the upper part with high ballast content, but floated in the 58 fines matrix for the lower part with lower ballast content. Since the ballast/fines 59 60 mixture plays an important role in the overall behaviour of rail tracks, it is important to investigate the mechanical response of such mixture under cyclic loading in terms 61 of permanent deformation and resilient modulus. Considering the large size of ballast 62 63 grains, large-scale triaxial apparatus is normally needed for this purpose. However, since the large testing system is complex and costly, scaling the ballast grains down to 64 a model ballast material with smaller size and performing tests using standard 65 apparatus appear quite promoting. 66

Three methods are commonly used for the scaling purpose: the scalping method [50] which consists in discarding the grains larger than a specified size from the prototype materials, the parallel gradation method [24] which consists in creating a model material at smaller size with its grain size distribution parallel to that of the

prototype material, and the replacement method [14] which consists in replacing the 71 grains from a specified size to the maximum size with the grains from this specified 72 73 size to a smaller size. Among them, the parallel gradation method is regarded to be the most appropriate because it can consider a large range of prototype gradation shape; 74 75 thus, it has been adopted mostly [1,16,29,39,42,43,44,47]. The validity of this method under cyclic loadings was assessed by Sevi and Ge [34] based on the response of the 76 prototype and model grains of ballast grains. Their results in terms of resilient 77 modulus, permanent axial strain and permanent volumetric strain were unfortunately 78 79 not conclusive for validating the parallel gradation method. In addition, only pure ballast grains were tested without fines fraction. 80

In this study, the parameters characterizing the cyclic response (permanent 81 82 strain and resilient modulus) of ballast/fines mixtures representing the interlayer soils in the conventional French railway track-beds were determined by conducting 83 large-scale cyclic triaxial tests. Six volumetric ballast contents (0%, 5%, 10%, 20%, 84 85 35%, 45%) were considered. The results obtained were analysed together with those obtained previously by Wang et al. [42,43] from small-scale cyclic triaxial tests on 86 microballast/fines mixture with microballast prepared by applying the parallel 87 gradation method. Comparison of the mechanical parameters obtained at two scales 88 allowed the validity of the parallel gradation method to be assessed on coarse 89 grain/fines mixtures. 90

#### 92 **2. Materials**

The ballast grains having the same grain size distribution as the interlayer soil in 93 "Sénissiat site" were used [37], as shown in Fig. 1. The minimum grain size  $D_{\min}^{b}$ 94 and the maximum grain size  $D_{\text{max}}^{b}$  are 20 mm and 63 mm, respectively. The 95 microballast was tested previously by Wang et al. [42,43]; its maximum grain size 96  $D_{\max}^m$  was chosen as 20 mm to adapt to a small-scale triaxial cell of 100 mm with a 97 value of 5 as the ratio of specimen to maximum grain size. This is consistent with the 98 recommendation of Fagnoul and Bonnechere [12], Nitchiporovitch [25] and Pedro 99 100 [28]: a ratio larger than 5 must be adopted to minimize the specimen size effect. The grain size distribution of the microballast is transited from that of the ballast by 101 following the parallel gradation method. In this method, the correlative grain sizes of 102 103 ballast and microballast share the same percentage of grain passing. The grain sizes of these two materials are correlated according to the following equation: 104

105 (1) 
$$\frac{D^b - D^b_{\min}}{D^m - D^m_{\min}} = \frac{D^b_{\max} - D^b_{\min}}{D^m_{\max} - D^m_{\min}} = A$$

where  $D_{\text{max}}$ ,  $D_{\text{min}}$  and D are the maximum grain size, the minimum grain size, and a given grain size, respectively. The superscripts b and m stand for ballast and microballast, respectively. A is a constant.

To prepare the microballast, three angular-shaped commercial coarse grains were used. Visually, the grain shape of the chosen commercial grains was similar to that of the field ballast from "Sénissiat site". The minimum grain size of the commercial grains  $D_{\min}^m$  was 1.6 mm, defining a value of 2.337 for parameter A. For a given grain size of microballast  $D^m$ , 10.0 mm for instance, equation (1) gives a 114 correlated ballast grain size  $D^b$  of 39.6 mm. As the ballast grain passing percentage 115 is 59.1 % for  $D^b = 39.6$  mm, according to the parallel gradation method, the 116 microballast grain passing percentage is also 59.1 % for  $D^m = 10$  mm. Following this 117 procedure, the complete grain size distribution of the microballast was obtained, as 118 shown in Fig. 1. This target (parallel gradation) curve was verified by measurement 119 and it is observed that the measured grain size distribution and the target one show a 120 good agreement (Fig. 1).

For the fines soils, since obtaining enough quantity from the field was difficult, 121 122 they were fabricated in the laboratory. Nine commercial soils were mixed to simulate the fines soils from "Sénissiat site", which included five kinds of medium sands, two 123 kinds of fine sands and two kinds of clay soils (kaolinite and bentonite). Table 1 listed 124 125 the properties of these soils. The mass proportion of each constituting soil was calculated according to the grain-size distributions of the fines from "Sénissiat site" 126 (Fig. 2). The calculated results were also shown in Table 1. With the proportion and 127 128 the grain size distribution of each soil, the grain size distribution of the fabricated fines can be calculated, which was plotted in Fig. 2 as well. During the mixing 129 procedure, the materials to be mixed were carefully added into the mixer following 130 the sequence of medium sands, water, fine sands, kaolinite and bentonite. The mass of 131 the added water corresponded to a small water content of 4% of the total mixed soils. 132 The aim of water addition was to prevent the small particles loss during the mixing, 133 occurring when fine sands, kaolinite and bentonite were dry mixed with others. 134 Bentonite was added last since it was the most reactive soil with water. With this 135

sequence, most kaolinite and bentonite particles were expected to be adhered to the 136 surface of sands. Using this procedure, a homogeneous mixture can be obtained [21]. 137 Wang et al. [42,43] also adopted this method when preparing specimens of 138 microballast and fines mixture. After preparation, the fabricated fines soil was 139 compared with the field one in terms of grain size distribution and plasticity. As can 140 be observed from Fig. 2, the grain size distribution of the fabricated fines showed a 141 good agreement with that of the in situ one. In addition, the liquid limit and the 142 plasticity index of the fabricated fines, which were 32% and 20%, respectively, 143 matched the target liquid limit (35.5%) and plasticity index (17.3%) well. This soil is 144 classified as lean clay (CL) according to ASTM D2487-11 [3]. Standard Proctor 145 compaction tests were carried out on the fines material following ASTM D698-12 [4]. 146 147 An optimum water content  $w_{opt-f} = 13.70\%$  and a maximum dry density  $\rho_{dmax-f} = 1.82$  $Mg/m^3$  were determined. 148

149

#### 150 **3. Experimental methods**

#### 151 **3.1. Specimen preparation**

In order to quantify the coarse grains in a specimen, a parameter namely volumetric content of coarse grains  $f_v$  was adopted, which was defined as the ratio of the total volume of coarse grains to the total specimen volume [28,29,32,42,43,44]. The total specimen volume consisted of two parts: the coarse grain volume and the fines volume. All pores were assumed to be included in the fines soils. For the upper part of the natural interlayer soils at "Sénissiat site", the  $f_v$  value was 52.9% [37]. In this study, six  $f_{\nu}$  values (0%, 5%, 10%, 20%, 35%, 45%) were considered for the specimens prepared with both ballast and microballast. For convenience, in further analysis, the specimens prepared with ballast and microballast are referred to as ballast specimens and microballast specimens, respectively. The dimensions of the ballast specimens are 300 mm diameter and 600 mm height, while the dimensions of microballast specimens are 100 mm diameter and 200 mm height.

For the preparation of the ballast specimen, the total volume was first calculated 164 with the specimen dimensions (300 mm diameter and 600 mm height). For a given  $f_{\nu}$ 165 166 value, the volumes of both ballast grains and fines can be obtained based on this total specimen volume. After that, the mass of ballast was obtained using the dry unit mass 167 of ballast (2.68 Mg/m<sup>3</sup>). The fines in all specimens were kept at the same state defined 168 169 by the optimum water content  $w_{opt-f} = 13.70\%$  and the maximum dry density  $\rho_{dmax-f} =$ 1.82 Mg/m<sup>3</sup>. The optimum state was selected aiming to simulate the heavily compact 170 state in the field condition [8,21,38]. Accordingly, the masses of dry fines and water 171 can be determined. Water was firstly added into the fines by spray to reach the 172 optimum water content  $w_{opt-f} = 13.7\%$ . Then, the wetted fines soil was stored in 173 hermetic containers for 24 h for moisture homogenization. Afterwards, the 174 homogenized wetted fines soil was equally divided into eight parts (by weight) and so 175 were the oven-dried ballast grains, after which they were mixed separately. Finally, 176 the ballast specimen was compacted using a layered compaction method, which was 177 widely adopted by many researchers to ensure reasonable uniformity of the specimen 178 [5,22,35,46]. The mixed materials were compacted in eight layers using a vibration 179

180 hammer, each with a thickness of 75 mm.

Similar protocol was applied for the preparation of the microballast specimen 181 182 (100 mm diameter and 200 mm height). The masses of the dry microballast, dry fines soil and water were firstly determined. Afterwards, the fines soil was wetted with the 183 sprayed water to reach the optimum water content of 13.7%, stored in hermetic 184 container for 24 h and then mixed with the microballast. Finally, this mixture was 185 compacted dynamically to reach the target height, also following the layered 186 compaction method to ensure reasonable uniformity of the specimen. More details can 187 188 be found in Wang et al. [42,43]. Note that the test results at five  $f_v$  values (5%, 10%, 20%, 35%, 45%) obtained by Wang et al. [42,43] were taken for comparison with the 189 190 corresponding ones of the ballast samples in this study.

191

#### 192 **3.2.** Cyclic triaxial tests

For the microballast specimen with 100 mm diameter and 200 mm height, a 193 small-scale cyclic triaxial apparatus was used. Details about this device can be found 194 in Wang et al. [43]. For testing a ballast specimen (300 mm diameter and 600 mm 195 height), a large-scale cyclic triaxial apparatus developed by Dupla et al. [11] was 196 adopted. The loading procedures adopted are the same for the ballast and the 197 microballast specimens. No saturation process was applied and the specimen water 198 content was kept constant during the test. In addition, the drainage valve was kept 199 open during the loading process. All the tests were performed at a confining pressure 200 of 30 kPa, which corresponded to the average horizontal stress estimated for the field 201

condition, considering the effects of the train wheel load, the interlayer depth and the 202 Poisson ratio [9,42,43]. The applied cyclic loads followed a sine-shaped pattern (Fig. 203 204 3). The deviator stress amplitude  $\Delta q$  is defined as the difference value between the maximum deviator stress  $q_{max}$  and the minimum deviator stress  $q_{min}$  [40,41,42,43]. A 205 frequency of 1.78 Hz corresponding to a low train speed of 50 km/h was chosen, 206 aiming to guarantee the quality of controlling the pre-defined loading shape. Note that 207 this low frequency did not reflect the high train speed normally encountered in the 208 field. This selection was based on the hypothesis that the train speed does not 209 210 influence the assessment of the validity of the parallel gradation. During the loading procedure, axial stress and strain were monitored. 211

The application of cyclic loads included two consecutive stages. The loading 212 213 stage 1 was focused on the aspect of the permanent deformation under a large number of loading cycles. The loading stage 2 was focused on the aspect of the resilient 214 modulus or stiffness property under a wide range of stress amplitudes, including some 215 large amplitudes possibly applied on the interlayer soils. In stage 1, a multi-step 216 loading procedure proposed by Gidel et al. [13] was adopted (Fig. 4a): the deviator 217 stress amplitude  $\Delta q = q_{max} - q_{min}$  was increased stepwise from 10 kPa to 30 kPa with 218 an increment of 5 kPa. At each amplitude, 90,000 cycles were applied, which were 219 thought to be enough for the stabilization of the permanent strain [10,13,21,38]. This 220 multi-stage loading procedure allowed the application of several stress amplitudes on 221 the same specimen, with which not only the number of tests could be reduced, but 222 also the effect of the variability of soil specimens on the testing results can be 223

224	minimised. Thus, this procedure has been widely used in the study of the permanent
225	deformation behaviour [6,10,19,21,36,38,43]. These loading amplitudes were selected
226	based on the vertical stress measured at the equivalent depth of interlayer in the field
227	[20,21]. In stage 2 (Fig. 4b), a procedure proposed by Lamas-Lopez [23] was adopted.
228	The deviator stress amplitude $\Delta q$ was firstly increased following a $\Delta q$ sequence (10
229	kPa, 30 kPa and 50 kPa) and then decreased following the reverse sequence.
230	Afterwards, $\Delta q$ was increased following a sequence from 10 kPa to 100 kPa and then
231	decreased to 10 kPa. Finally, $\Delta q$ was increased in steps to 200 kPa and then decreased
232	to 10 kPa. At each stress level, 100 cycles were applied. The aim of firstly increasing
233	$\Delta q$ and then decreasing it was to obtain the resilient modulus at both elastoplastic
234	stage and pure elastic stage. Note that the large stress amplitudes (50 kPa, 100 kPa
235	and 200 kPa) were defined according to the vertical stress of 40-90 kPa at similar
236	depth of the interlayer observed by Selig and Waters [33], Jain and Keshav [18] and
237	Yang et al. [49], the vertical stress of 120-138 kPa applied by heavier wagons in some
238	countries [15,18,23] and the contingent maximum vertical stress at the top of railway
239	structure as high as 200 kPa [21].

240

#### 241 **4. Results and discussions**

#### 242 **4.1.** Variations of permanent deformation with $f_v$

Fig. 5 plots the deviator stress q versus the axial strain  $\varepsilon_1$  during the first 90,000 cycles of loading stage 1 for the ballast specimen at  $f_v = 35\%$ . In a loading-unloading cycle, the permanent axial strain  $\varepsilon_{1p}$  represented the irreversible part of the total 246 axial strain. It can be observed that the  $\varepsilon_{1p}$  value of the first cycle was particularly large. This phenomenon was also observed for other ballast specimens and the 247 microballast specimens. This large permanent strain can be attributed to the 248 adaptation of the specimen to the loading system, in particular in terms of contact 249 between the specimen and the loading piston. As the initial specimen-piston contact 250 251 was not identical for all the specimens, this  $\varepsilon_{1p}$  value would make impossible the relevant comparison of permanent strain between different specimens. Thus, in further 252 analysis, the first cycle was not accounted for the cumulative permanent strain. 253

Fig. 6 presents the permanent strain  $\varepsilon_{1p}$  against the number of cycles N for six 254 ballast specimens, with the corresponding stress levels. The evolutions of permanent 255 strain with number of cycles N were the same as the ones of microballast specimens 256 257 [43]. It can be observed from Fig. 6 that for each  $f_v$  value,  $\varepsilon_{1p}$  increased quickly at the start of each loading level and then tended to stabilize with the increasing cycles. 258 According to Werkmeister et al. [45], the large deformation in the beginning resulted 259 260 from a significant rearrangement of the particles. As the cycle number increased, this 261 particle rearrangement became more and more limited, and correspondingly, the permanent strain tended to become stable. As can also be seen from Fig. 6, a 262 smaller  $f_v$  value led to a larger  $\varepsilon_{1p}$ , which can be attributed to the involvement of less 263 264 coarse grains.

Due to the multi-step loading procedure adopted, the  $\varepsilon_{1p}$  at each stress level was greatly influenced by the previous loadings (Fig. 6). If this loading history is eliminated (as if the specimen has been subjected to only one loading level), the effect of the ballast contents can be better evaluated. For this purpose, a permanent strain estimation method proposed by Gidel et al. [13] and then used by Lamas-Lopez [21] and Wang et al. [43] was adopted. The application of this method is explained in Fig. 7 by considering two successive loading levels (Loading level *M* and Loading level *M* + 1). For the estimated permanent strain  $\varepsilon_{1p}^{M+1}$  of the Loading level *M* + 1 at the first 90,000 cycles, it is determined as:

274 (2) 
$$\varepsilon_{1p}^{M+1} = \varepsilon_{1p}^{M} + \delta \varepsilon_{1p}^{M+1}$$

where  $\varepsilon_{1p}^{M}$  is the measured permanent strain of the Loading Level *M*;  $\delta \varepsilon_{1p}^{M+1}$  is the translated permanent strain determined by resetting both the initial strain value and the first cycle of the measured permanent strain of the Loading level *M* + 1 to 0.

For estimating the permanent strain of the Loading level M + 1 after 90,000 cycles, a linear increasing trend between permanent strain and number of cycles is considered, with its slope kept at the same value as the one determined at the last cycles of Loading level M + 1. More details can be found in Wang et al. [43].

The estimated permanent strain curves for  $f_v = 0\%$  of the ballast specimen are 282 presented in Fig. 8, together with the measured results. It can be observed that at the 283 last cycle of each stress level, the estimated strain was larger than the measured one. 284 For example, for  $\Delta q = 20$  kPa, the measured permanent strain at the last cycle N = 285 270,000 was 0.182%, while the corresponding estimated one was 0.226%. This 286 phenomenon can be attributed to the different loading histories: for the estimated 287 strain, the specimen was assumed to undergo one higher stress level of 20 kPa. When 288 it came to the measured strain, successive lower stress levels of 10kPa, 15 kPa and 20 289

kPa were applied, leading to a smaller strain value.

Gidel et al. [13] examined this permanent strain estimation method through 291 292 cyclic triaxial tests, concluding that the permanent strain estimated for a single stress level agreed well with the measured one for the loading cycles applied at each step 293 (90,000 cycles in this study). In other words, in this study, the estimated permanent 294 strain at the first 90,000 cycles was relatively accurate. Fig. 9 depicts the estimated 295 permanent strain evolutions at the first 90,000 cycles under different stress levels for 296 ballast specimen at  $f_v = 0\%$ . As can be observed, a larger stress level led to a larger 297 298 strain value. In addition, the permanent strain gradually stabilized with the increase of the cycle number. To further illustrate the effect of ballast content  $f_{\nu}$ , the estimated 299 permanent strains for cycle N = 90,000 (end-stage cycle in Fig. 9) at all stress levels 300 301 were taken and compared (Fig. 10). It can be observed that at each stress level, the permanent strain decreased with the increase of  $f_{\nu}$ . Moreover, a bi-linear decreasing 302 trend could be identified. When  $f_v \leq 20\%$ , the permanent strain decreased rapidly. By 303 304 contrast, when  $f_v \ge 35\%$ , this decreasing rate became smaller. The same observations were made by Wang et al. [43] for the microballast specimens. 305

In the study of Wang et al. [43], X-ray microcomputed tomography ( $\mu$ CT) scans were carried out on the as-compacted microballast specimens. Two soil fabrics were identified at different  $f_v$  values: a fine-fine contact structure at  $f_v = 0\%$ -20% and a distinct grain-grain contact structure at  $f_v = 35\%$ -45%. It is worth noting that at  $f_v =$ 20%, the coarse grains started to be partially connected without forming a whole skeleton. Unfortunately, this  $\mu$ CT scan could not be conducted on ballast specimens due to their large size. However, basically, it seems plausible to consider the same feature of fabrics for the ballast specimens: also a fine-fine contact structure at low  $f_v$ and a grain-grain contact structure at high  $f_v$ . For fine-fine contact structure, the permanent strain results from the compression of the fines, which decreases rapidly with increasing  $f_v$ . By contrast, for grain-grain contact structure, the rearrangement of the grains plays a dominant role and the permanent strain decreases slightly when  $f_v$ increases.

319

#### 320 **4.2.** Variations of resilient modulus with $f_v$

Typical hysteresis loops at the first cycles of different stress levels are shown in Fig. 321 11 for the ballast specimen at  $f_v = 20\%$ . The loops for stress levels of  $\Delta q = 10$  kPa,  $\Delta q$ 322 323 = 30 kPa,  $\Delta q$  = 50 kPa,  $\Delta q$  = 100 kPa and  $\Delta q$  = 200 kPa corresponded to cycle numbers of N = 1, N = 101, N = 201, N = 701 and N = 1401, respectively. It appears 324 that for the low stress levels of 10 kPa and 30 kPa, the hysteresis loops were pretty 325 small and closed. This was due to the application of 450,000 loading cycles under  $\Delta q$ 326  $\leq$  30 kPa in loading stage 1. By contrast, for stress levels larger than 30 kPa, 327 permanent strain developed, leading to larger and unclosed hysteresis loops, in 328 particular under stress levels as high as  $\Delta q = 100$  kPa and 200 kPa. 329

The evolution of hysteresis loop with number of cycles is illustrated in Fig. 12 by plotting the loops for 100 cycles (from N = 701 to N = 800) at  $\Delta q$  = 100 kPa for the ballast specimen with  $f_v$  = 20%. A large and unclosed hysteresis loop was observed for the first cycle, due to the stress level of 100 kPa which was larger than all the previous applied stress levels. In addition, with the increase of the cycle number, the hysteresis loop became smaller and smaller and at the end of loading, the loops became closed and relatively unchanged, suggesting a pure elastic behaviour of soil.

As shown in Fig. 13, the resilient modulus  $M_r$  is defined as [30,31]:

337

338

$$(3) M_r = \Delta q / \varepsilon_1$$

where  $\Delta q$  is the deviator stress amplitude, and  $\varepsilon_{1r}$  is the resilient strain.

The evolution of  $M_r$  with the number of cycles N at varying stress levels is 340 presented in Fig. 14 for the ballast specimen at  $f_v = 20\%$ . The results of other ballast 341 342 specimens and microballast specimens obey the same rule and are not shown for clarity. It can be observed that when the stress amplitude increased, the  $M_r$  value 343 immediately decreased and then tended to stabilize. By contrast, with the stress 344 345 amplitude decreasing, the  $M_r$  value increased instantly and then tended to reach a stabilization state. The decrease of  $M_r$  with the increase of stress amplitude can be 346 explained by the strain increasing due to the increase of stress amplitude [2]. 347

348 In order to illustrate the effect of  $f_v$  on resilient modulus, the  $M_r$  values of the last (end-stage) cycles of all stress levels were taken and presented as a function of  $f_{\nu}$ 349 for different stress levels (Fig. 15). The data were named according to the number of 350 cycles N and the corresponding  $\Delta q$  values. It appears that an increasing trend of  $M_r$ 351 with  $f_v$  can be identified for all stress levels. Moreover, this increasing trend followed 352 a bi-linear pattern with the slope at  $f_v \ge 35\%$  larger than the one at  $f_v \le 20\%$ , 353 evidencing that the soil fabrics of the ballast specimens at these two  $f_v$  ranges were 354 different: fine-fine contact structure at low  $f_{\nu}$  and grain-grain contact structure at 355

higher  $f_{\nu}$ . Same bi-linear variation trend of  $M_r$  was identified by Wang et al. [42] for the microballast specimens, similarly, evidencing that the soil fabrics of microballast specimens at  $f_{\nu} \le 20\%$  and  $f_{\nu} \ge 35\%$  were separately dominated by fine-fine contact structure and grain-grain contact structure.

360

# 4.3. Comparison of permanent strain between ballast and microballast specimens

The estimated permanent strains for cycle N = 90,000 (end-stage cycle) at six  $f_v$  values 363 are presented in Fig. 16 for the ballast and the microballast specimens, for five stress 364 levels (10, 15, 20, 25 and 30 kPa). It can be observed that in the case of  $f_v = 0\%$ , at 365 each stress level, the  $\varepsilon_{1p}$  value of the ballast specimen coincides well with that of the 366 microballast specimen. For the fine-fine contact structure at  $f_v = 5\%$  and 10%, on the 367 whole, the  $\varepsilon_{1p}$  values of the corresponding different scale specimens are found to be 368 similar. This phenomenon can be explained by the fact that in this case the fines 369 matrix constitutes the soil skeleton and the permanent strain was dominated by the 370 compression of the fines, giving rise to the permanent strains which were independent 371 of coarse grain size. For the grain-grain contact structure at  $f_v = 35\%$  and 45%, it can 372 be observed that the permanent strains of the ballast specimens and the microballast 373 specimens were almost the same (Fig. 16), in particular at  $\Delta q = 10$  kPa (Fig. 16a). 374 Note that although the case at  $f_v = 20\%$  was categorized into the group of fine-fine 375 contact structure, the influence of coarse grain size on the permanent strain followed 376 the same pattern. This can be explained by the fact that at  $f_v = 20\%$ , part of the coarse 377

grains started to be in contact with each other. Further examination shows that at  $\Delta q$ 378 higher than 10 kPa, the strains of microballast specimens were slightly larger than 379 380 those of the ballast specimens. This phenomenon can be explained as follows: upon loadings, the grains would slide into the pores nearby, giving rise to permanent strain. 381 If the difficulty of sliding into large pores for the large grains was the same as that for 382 the smaller grains to slide into smaller pores, identical permanent strains can be 383 expected. It is the case for the ballast specimen and the microballast specimen at  $\Delta q =$ 384 10 kPa. Apparently, the grains sliding depended on the stress level and the grain sizes; 385 386 in the microballast specimen, the grains with smaller sizes would slide into the adjacent pores more easily, leading to a slightly larger strain. 387

Another possible explanation for the slightly larger strains in the microballast 388 389 specimen is related to the effect of the fines soils. As shown in Fig. 17, the fines soils can be roughly considered to be distributed at two locations: the pores near the coarse 390 grain and the coarse grain intervals along the stress chain (supposed to be along the 391 specimen height). The applied load was transmitted along the stress chain by 392 compressing the fines between grains. When the load reached a certain level, grain 393 rearrangement occurred [26,27]. It can be inferred that the fines in the pores inhibited 394 the coarse grain sliding, while those between grains promoted it. At a given  $f_v$  value, 395 for the microballast specimen, more grain-fines-grain contacts can be expected along 396 the stress chain, leading to more distribution of fines soils. As a result, relatively 397 larger permanent strain can be expected. 398

399

As the difference of permanent strain between the two scale specimens appears

quite small (Figure. 16), it can be reasonably concluded that the parallel gradationmethod is valid for the ballast/fines mixture in terms of permanent strain.

402

# 403 **4.4. Comparison of resilient modulus between ballast and microballast specimens** 404 The comparison of $M_r$ values between the microballast and ballast specimens with 405 fine-fine contact structure is shown in Fig. 18. At $f_v = 0\%$ , the $M_r$ values of the ballast 406 specimen were comparable with those of the microballast specimen. This was normal 407 because the scaling question wasnot involved in that case. For higher $f_v$ values, except 408 $f_v = 10\%$ , the $M_r$ values of the ballast and the microballast specimens coincided with 409 each other. The singular case at $f_v = 10\%$ was probably due to a technical problem.

The  $M_r$  values of the ballast specimens at grain-grain contact structure were 410 compared with those of the mciroballast specimens in Fig. 19 (Fig. 19a for  $f_v = 35\%$ 411 and Fig. 19b for  $f_v = 45\%$ ). It can be observed that almost the same  $M_r$  values were 412 obtained for the two specimens, indicating that the resilient modulus was independent 413 of grain size. Further investigation shows that on the whole the  $M_r$  values of the 414 microballast specimens were slightly smaller than those of the ballast specimens. 415 These phenomena can be explained based on the analysis of Yang and Gu [48]. They 416 derived the resilient modulus of a simple cubic array of identical spheres under a 417 certain confining pressure by applying a small shear stress onto it. In the analysis, the 418 induced resilient shear strain of the cubic array was determined by adding up the 419 tangential strains between every two spheres along the vertical stress chain. This 420 tangential strain was calculated using the Hertz-Mindlin contact law, which was a 421

function of the applied shear stress. The expression for the resilient modulus (defined as the ratio of the shear stress to the shear strain) was obtained, showing no dependence on sphere radius. Note that this analysis did not consider any contribution from fine soils, thus not fully reflecting the case of this study. Indeed, as mentioned previously, in the case of mixture, the resilient modulus is affected by the fine soils along the stress chain. For the microballast specimens, as stated before, there are more fines soils along it. Thus, relatively smaller resilient modulus values are expected.

As for the permanent strain, globally, the resilient modulus also showed a good agreement between the two scale specimens albeit the slight difference discussed above, which validates the parallel gradation method in terms of resilient modulus.

432

#### 433 **5.** Conclusions

The parallel gradation method was assessed on coarse grain/fines mixture by comparing the mechanical parameters (permanent strain and resilient modulus) of the two different scale specimens. Six volumetric coarse grain contents were considered for each kind of specimens. Based on the results obtained, the following conclusions can be drawn.

Two soil fabrics could be defined as fine-fine contact structure at  $f_v = 0.20\%$ and grain-grain contact structure at  $f_v = 35.45\%$ . It was observed that for the ballast and microballast specimens, with the increase of  $f_v$  value, the permanent strain decreased rapidly when  $f_v \le 20\%$  and this decreasing rate slowed down when  $f_v \ge 35\%$ , while the resilient modulus increased slightly when  $f_v \le 20\%$  and increased 444 significantly when  $f_v \ge 35\%$ .

445	The consistency between the large-scale and small-scale triaxial tests were
446	found to be satisfactory: at $f_v = 0\%$ , the permanent strain as well as the resilient
447	modulus values obtained from the two scales showed a good correspondence. In the
448	case of fine-fine contact structure, the parallel gradation method was found to be valid.
449	The permanent strain and resilient modulus values of the ballast specimens were
450	consistent with the respective ones of the microballast specimens. This could be
451	explained by the fact that in this case the fines matrix governed the soil structure.
452	In the case of grain-grain contact structure, on the whole, the permanent strains
453	of the ballast specimens coincided with those of the microballast specimens
454	(especially at $\Delta q = 10$ kPa). This coincidence was also observed in terms of resilient
455	modulus. For the permanent strain, it could be explained by the fact that the
456	difficulties of the sliding of large ballast grains into the adjacent large pores and the
457	sliding of the small microballast grains into the smaller pores were expected to be the
458	same. For the resilient modulus, it could be explained by the analytical results of Yang
459	and Gu (2013), showing that the resilient modulus is independent of grain size.
460	Further examination showed that there were slight differences of permanent strain and
461	resilient modulus between two different scale specimens, which could be attributed to
462	the irregular grain sliding and the fines distribution.

463

#### 464 Acknowledgements

465 The support from the Chinese Scholar Council (CSC) is greatly acknowledged.

#### 467 Notations

A	constant in the similitude equation from ballast to microballast
$D^b$	given grain size of ballast
$D_{\max}^b$	maximum grain size of ballast
$D^b_{\min}$	minimum grain size of ballast
$D^m$	given grain size of microballast
$D_{\max}^m$	maximum grain size of microballast
$D_{\min}^m$	minimum grain size of microballast
$f_v$	volumetric content of coarse grains
$M_r$	resilient modulus
Ν	number of cycles
q	deviator stress
$q_{max}$	maximum deviator stress
$q_{min}$	minimum deviator stress

Wopt-f	optimum water content of fines
$\Delta q$	deviator stress amplitude
$\delta arepsilon_{1p}^{M+1}$	translated permanent strain from the measured curve of Loading level
	M+1
$\varepsilon_1$	axial strain

$\varepsilon_{1p}$	permanent axial strain
$\varepsilon_{1r}$	resilient strain
$\varepsilon^M_{1p}$	measured permanent strain of the Loading Level M
$\varepsilon_{1p}^{M+1}$	estimated permanent strain of Loading level M+1
$ ho_{ m dmax-f}$	maximum dry density of fines

469 **References** 

- [1] Aingaran, S. 2014. Experimental investigation of static and cyclic behavior of
  scaled railway ballast and the effect of stress reversal. Ph.D. thesis, University of
  Southampton.
- 473 [2] Atkinson, J.H. 2000. Non-linear soil stiffness in routine design. Géotechnique,
  474 50(5): 487-507.
- [3] ASTM. 2011. D2487-11: Standard practice for classification of soils for
  engineering purposes (unified soil classification system). ASTM International,
  West Conshohocken, PA, USA.
- [4] ASTM. 2012. D698-12: Standard test methods for laboratory compaction
  characteristics of soil using standard effort. ASTM International, West
  Conshohocken, PA, USA.
- 481 [5] Cai, Y.Q., Chen, J.Y., Cao, Z.G., Gu, C., and Wang, J. 2018. Influence of grain
- gradation on permanent strain of unbound granular materials under low confining
- 483 pressure and high-cycle loading. International Journal of Geomechanics, 18(3):

484 04017156.

485	[6] Cao, Z.G., Chen, J.Y., Cai, Y.Q., Zhao, L., Gu, C., and Wang, J. 2018. Long-term
486	behavior of clay-fouled unbound granular materials subjected to cyclic loadings
487	with different frequencies. Engineering Geology, 243: 118-127.
488	[7] Cui, Y.J., Duong, T.V., Tang, A.M., Dupla, J.C., Calon, N., and Robinet, A. 2013.
489	Investigation of the hydro-mechanical behavior of fouled ballast. Journal of
490	Zhejiang University-Science A (Applied Physics & Engineering), 14(4): 244-255.
491	[8] Duong, T.V. 2013. Investigation of the hydro-mechanical behavior of ancient
492	railway platforms in scope to reinforcement by soil-mixing. Ph.D. thesis, Ecole
493	Nationale des Ponts et Chaussées, Université Paris-Est.
494	[9] Duong, T.V., Cui, Y.J., Tang, A.M., Dupla, J.C., Canou, J., Calon, N., and Robinet,
495	A. 2016. Effects of water and fines contents on the resilient modulus of the
496	interlayer soil of railway substructure. Acta Geotechnica, 11(1): 51-59.
497	[10] Duong, T.V., Tang, A.M., Cui, Y.J., Trinh, V.N., Dupla, J.C., Calon, N., Canou, J.,
498	and Robinet, A. 2013. Effects of fines and water contents on the mechanical
499	behavior of interlayer soil in ancient railway sub-structure. Soils and Foundations,
500	53(6): 868-878.
501	[11] Dupla, J.C., Pedro, L.S., Canou, J., and Dormieux, L. 2007. Mechanical behavior
502	of coarse grained soils reference. Bulletin de Liaison des Laboratoires des Ponts
503	et Chaussées, 268-269: 31-58.
504	[12] Fagnoul, A., and Bonnechere, F. 1969. Shear strength of porphiry materials. In

505 Proceedings of the 7th International Conference on Soil Mechanics and506 Foundation Engineering, Mexico, pp. 61-65.

507	[13] Gidel, G., Hornych, P., Chauvin, J.J., Breysse, D., and Denis, A. 2001. A new
508	approach for investigating the permanent deformation behavior of unbound
509	granular material using the repeated load triaxial apparatus. Bulletin des
510	Laboratoires des Ponts et Chaussées, 233: 5-21.

- [14] Frost, R.J. 1973. Some testing experiences and characteristics of boulder-gravel
  fills in earth dams. *In* Evaluation of relative density and its role in geotechnical
  projects involving cohesionless soils. STP 523. ASTM Standards and
  Publications.
- [15] Grabe, P., and Clayton, C. 2009. Effects of principal stress rotation on permanent
  deformation in rail track foundations. Journal of Geotechnical and
  Geoenvironmental Engineering, 135(4): 555–565.
- 518 [16] Indraratna, B., Wijewardena, L.S.S., and Balasubramaniam, A.S. 1993.
  519 Large-scale triaxial testing of greywacke rockfill. Géotechnique, 43: 37-51.
- [17] Indraratna, B., Su, L., and Rujikiatkamjorn, C. 2011. A new parameter for
  classification and evaluation of railway ballast fouling. Canadian Geotechnical
- 522 Journal, 48(2): 322-326.
- [18] Jain, V., and Keshav, K. 1999. Stress distribution in railway formation a
   simulated study. *In* Proceeding of the 2<sup>nd</sup> International Symposium on Pre-Failure
   Deformation Characteristics of Geomaterials-IS Torino.
- 526 [19] Jing, P., Nowamooz, H., and Chazallon, C. 2016. Permanent deformation
  527 behaviour of a granular material used in low-traffic pavements. Road Materials
  528 and Pavement Design, 19(2): 289-314.

529	[20] Lamas-Lopez, F., Costa D'Aguiar, S., Robinet, A., Cui, Y.J., Calon, N., Canou, J.,
530	Dupla, J.C., and Tang, A.M. 2015. In-situ investigation of the behaviour of a
531	French conventional railway platform. In Proceedings of Transportation Research
532	Board TRB 2015, Washington, DC.
533	[21] Lamas-Lopez, F. 2016. Field and laboratory investigation on the dynamic
534	behaviour of conventional railway track-bed materials in the context of traffic

- upgrade. Ph.D. thesis, Ecole Nationale des Ponts et Chaussées, Université
  Paris-Est.
- [22] Lenart, S., Koseki, J., Miyashita, Y., and Sato, T. 2014. Large-scale triaxial tests
  of dense gravel material at low confining pressures. Soils and Foundation, 54(1):
  45-55.
- 540 [23] Li, D., and Selig, E. 1998. Method for railroad track foundation design. I:
  541 Development. Journal of Geotechnical and Geoenvironmental Engineering,
  542 124(4): 316–322.
- [24] Lowe, J. 1964. Shear strength of coarse embankment dam materials. *In*Proceedings of the 8th International Congress on Large Dams 3, Edinburgh, U.K.,
  pp. 745-761.
- [25] Nitchiporovitch, A.A. 1969. Shearing strength of coarse shell materials. *In*Proceedings of the 7th International Conference on Soil Mechanics and
  Foundation Engineering, Mexico, pp. 211-216.
- 549 [26] Oda, M., Konishi, J., and Nasser, N.S. 1982. Experimental micromechanical
  550 evaluation of strength of granular materials: effects of particle rolling. Mehcanics

- of Materials, 1(4): 269-283.
- 552 [27] Oda, M., and Kazama, H. 1998. Microstructure of shear band and its relation to
- the mechanisms of dilatancy and failure of dense granular soils. Géotechnique,
  48(4): 465-481.
- [28] Pedro, L. 2004. De l'étude du comportement mécanique de sols hétérogènes
  modèles à son application au cas des sols naturels. Ph.D. thesis, Ecole Nationale
  des Ponts et Chaussées, Université Paris-Est.
- 558 [29] Qi, S., Cui, Y.J., Chen, R.P., Wang, H.L., Lamas-Lopez, F., Aimedieu, P., Dupla,
- J.C., Canou, J., and Saussine, G. 2019. Influence of grain size distribution of
  inclusions on the mechanical behaviors of track-bed materials. Géotechnique in
  press. doi : 10.1680/jgeot.18.P.047.
- [30] Rollins, K.M., Evans, M.D., Diehl, N.B., and Daily III, W.D. 1998. Shear
  modulus and damping relationships for gravels. Journal of Geotechnical and
  Geoenvironmental Engineering, 124(5): 396-405.
- [31] Seed, H.B., Wong, R.T., Idriss, I.M., and Tokimatsu, K. 1986. Moduli and
  damping factors for dynamic analyses of cohesionless soils. Journal of
  Geotechnical Engineering, 112(11): 1016-1032.
- 568 [32] Seif El Dine, B., Dupla, J.C., Frank, R., Canou, J., and Kazan, Y. 2010.
- Mechanical characterization of matrix coarse-grained soils with a large-sized
  triaxial device. Canadian Geotechnical Journal, 47: 425-438.
- 571 [33] Selig, E., and Waters, J. 1994. Track geotechnology and sub-structure
  572 management. Thomas Telford, London, U.K.

573	[34] Sevi, A., and Ge, L. 2012. Cyclic behaviors of railroad ballast within the parallel
574	gradation scaling framework. Journal of Materials in Civil Engineering, 24(7):
575	797-804.

- 576 [35] Suiker, A.S.J., Selig, E.T., and Frenkel, R. 2005. Static and cyclic triaxial testing
- 577 of ballast and subballast. Journal of Geotechnical and Geoenvironmental 578 Engineering, 131: 771-782.
- [36] Tang, L., Yan, M.H., Ling, X.Z., and Tian, S. 2017. Dynamic behaviours of
  railway's base course materials subjected to long-term low-level cyclic loading:
  experimental study and empirical model. Géotechnique, 67(6): 537-545.
- [37] Trinh, V.N. 2011. Comportement hydromécanique des matériaux constitutifs de
  plateformes ferroviaires anciennes. Ph.D. thesis, Ecole Nationale des Ponts et
  Chaussées, Université Paris-Est.
- [38] Trinh, V.N., Tang, A.M., Cui, Y.J., Dupla, J.C., Canou, J., Calon, N., Lambert, L.,
- Robinet, A., and Schoen, O. 2012. Mechanical characterisation of the fouled
  ballast in ancient railway track sub-structure by large-scale triaxial tests. Soils
- 588 and Foundations, 52(3): 511-523.
- 589 [39] Varadarajan, A., Sharma, K.G., Venkatachalam, K., and Gupta, A.K. 2003.
- 590 Testing and modeling two rockfill materials. Journal of Geotechnical and 591 Geoenvironmental Engineering, 129(3): 206-218.
- [40] Wang, H.L., and Chen, R.P. 2019. Estimating static and dynamic stresses in
  geosynthetic-reinforced pile-supported track-bed under train moving loads.
  Journal of Geotechnical and Geoenvironmental Engineering, 145(7): 04019029.

595	[41] Wang, H.L., Chen, R.P., Cheng, W., Qi, S., and Cui, Y.J. 2019. Full-scale model
596	study on variations of soil stress in geosynthetic-reinforced pile-supported
597	track-bed with water level change and cyclic loading. Canadian Geotechnical
598	Journal, 56(1): 60–68.

- [42] Wang, H.L., Cui, Y.J., Lamas-Lopez, F., Dupla, J.C., Canou, J., Calon, N.,
  Saussine, G., Aimedieu, P., and Chen, R.P. 2017. Effects of inclusion contents on
  resilient modulus and damping ratio of unsaturated track-bed materials. Canadian
  Geotechnical Journal, 54: 1672-1681.
- [43] Wang, H.L., Cui, Y.J., Lamas-Lopez, F., Dupla, J.C., Canou, J., Calon, N.,
  Saussine, G., Aimedieu, P., and Chen, R.P. 2018a. Permanent deformation of
  track-bed materials at various inclusion contents under large number of loading
  cycles. Journal of Geotechnical and Geoenvironmental Engineering, 144(8):
  04018044.
- [44] Wang, H.L., Cui, Y.J., Lamas-Lopez, F., Calon, N., Saussine, G., Dupla, J.C.,
  Canou, J., Aimedieu, P., and Chen, R.P. 2018b. Investigation on the mechanical
  behavior of track-bed materials at various contents of coarse grains. Construction
  and Building Materials journal, 164: 228-237.
- [45] Werkmeister, S., Dawson, A.R., and Wellner, F. 2004. Pavement design model for
  unbound granular materials. Journal of Transportation Engineering, 130:
  665-674.
- [46] Wichtmann, T., Rondon, H.A., Niemunis, A., Triantafyllidis, Th., and Lizcano, A.
  2010. Prediction of permanent deformations in pavements using a high-cycle

- 617 accumulation model. Journal of Geotechnical and Geoenvironmental Engineering,618 136: 728-740.
  - [47] Xiao, Y., Liu, H.L., Chen, Y.M., and Jiang, J.S. 2014. Bounding surface model
  - for rockfill materials dependent on density and pressure under triaxial stressconditions. Journal of Engineering Mechanics, 140: 04014002.
  - [48] Yang, J., and Gu, X.Q. 2013. Shear stiffness of granular material at small strains:
    does it depend on grain size?. Géotechnique, 63(2): 165-179.
  - [49] Yang, L., Powrie, W., and Priest, J. 2009. Dynamic stress analysis of a ballasted
  - railway track bed during train passage. Journal of Geotechnical andGeoenvironmental Engineering, 135(5): 680–689.
  - [50] Zeller, J., and Wullimann, R. 1957. The shear strength of the shell materials for
    the Göschenenalp Dam, Switzerland. *In* Proceedings of the 4th International
    Conference on Soil Mechanics and Foundation Engineering, London, pp.
    399-404.

#### List of tables

Table 1. Mass proportions and grain size ranges of nine commercial soils

#### **List of Figures**

Fig. 1. Grain size distributions of the ballast and the microballast (modified from Wang et al. 2018a)

Fig. 2. Grain size distributions of fines (modified from Wang et al. 2018a)

Fig. 3. Typical sine-shaped signals applied in the cyclic loadings

Fig. 4. Loading paths in two stages: (a) stage 1 for permanent strain investigation; (b) stage 2 for resilient modulus investigation

Fig. 5. Deviator stress q versus axial strain  $\varepsilon_1$  for the first 90,000 cycles of loading stage 1 (ballast specimen at  $f_v = 35\%$ )

Fig. 6. Permanent strain evolutions with number of cycles at different  $f_v$  values (ballast specimens)

Fig. 7. Illustration of the method to eliminate the loading history effect

Fig. 8. Measured and estimated permanent strain curves for ballast specimen at  $f_v = 0\%$ 

Fig. 9. Estimated permanent strain evolutions at the first 90,000 cycles for ballast specimen at  $f_v = 0\%$ 

Fig. 10. Variations of estimated end-stage permanent strains with  $f_v$  at different stress levels (ballast specimens)

Fig. 11. Hysteresis loops at first cycles of different stress levels for ballast specimen at

 $f_v = 20\%$ :  $\Delta q = 10$  kPa (N = 1),  $\Delta q = 30$  kPa (N = 101),  $\Delta q = 50$  kPa (N = 201),  $\Delta q = 10$ 

100 kPa (N = 701) and  $\Delta q = 200$  kPa (N = 1401)

Fig. 12. Hysteresis loops during 100 cycles (N = 701 to 800) under  $\Delta q = 100$  kPa for ballast specimen at  $f_v = 20\%$ 

Fig. 13. Determination of  $M_r$ 

Fig. 14. Evolution of  $M_r$  with number of cycles at different stress levels for ballast specimen at  $f_v = 20\%$ 

Fig. 15. Evolutions of  $M_r$  at end stage with  $f_v$  for ballast specimens at: (a)  $\Delta q = 10$  kPa; (b)  $\Delta q = 30$  kPa; (c)  $\Delta q = 50$  kPa; (d)  $\Delta q = 100$  kPa and 200 kPa

Fig. 16. Variations of estimated end-stage permanent strains with  $f_{\nu}$  for ballast and microballast specimens at: (a)  $\Delta q = 10$  kPa; (b)  $\Delta q = 15$  kPa; (c)  $\Delta q = 20$  kPa; (d)  $\Delta q$ = 25 kPa and 30 kPa

Fig. 17. Schematic illustration of the distribution of fines soils in case of grain-grain contact structure

Fig. 18. Comparison of  $M_r$  value between ballast specimens and microballast specimens in case of fine-fine contact structure for: (a)  $f_v = 0\%$ ; (b)  $f_v = 5\%$ ; (c)  $f_v = 10\%$ ; (d)  $f_v = 20\%$ 

Fig. 19. Comparison of  $M_r$  value between ballast specimens and microballast specimens in case of grain-grain contact structure for (a)  $f_v = 35\%$  and (b)  $f_v = 45\%$ 

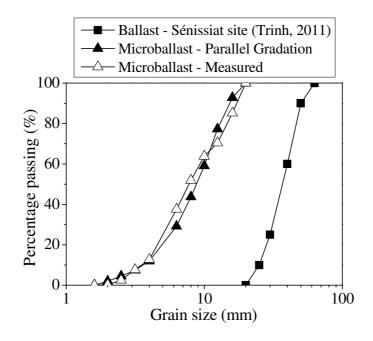


Fig. 1. Grain size distributions of the ballast and the microballast (modified from

Wang et al. 2018a)

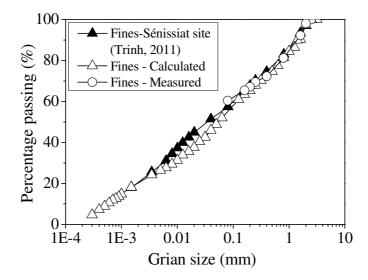


Fig. 2. Grain size distributions of fines (modified from Wang et al. 2018a)

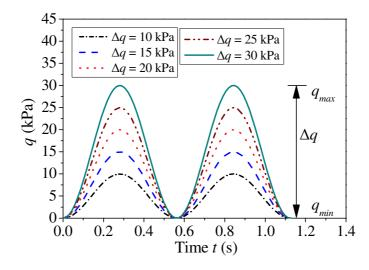


Fig. 3. Typical sine-shaped signals applied in the cyclic loadings

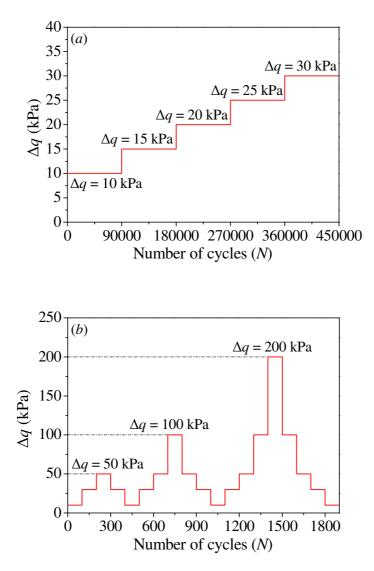


Fig. 4. Loading paths in two stages: (a) stage 1 for permanent strain investigation; (b)

stage 2 for resilient modulus investigation

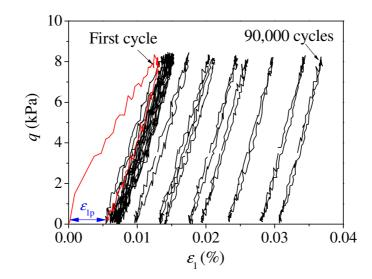


Fig. 5. Deviator stress q versus axial strain  $\varepsilon_1$  for the first 90,000 cycles of loading

stage 1 (ballast specimen at  $f_v = 35\%$ )

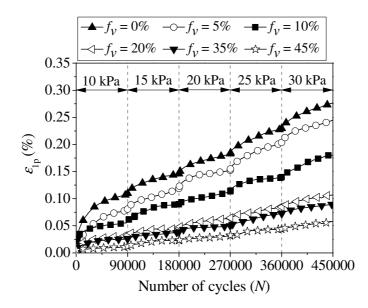


Fig. 6. Permanent strain evolutions with number of cycles at different  $f_v$  values

(ballast specimens)

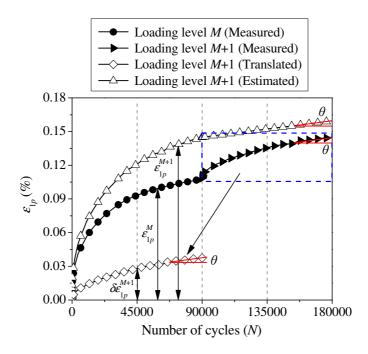


Fig. 7. Illustration of the method to eliminate the loading history effect

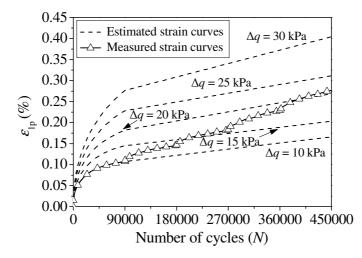


Fig. 8. Measured and estimated permanent strain curves for ballast specimen at  $f_v$  =



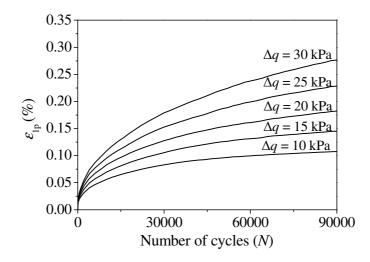


Fig. 9. Estimated permanent strain evolutions at the first 90,000 cycles for ballast

specimen at  $f_v = 0\%$ 

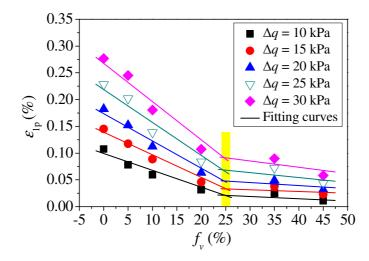


Fig. 10. Variations of estimated end-stage permanent strains with  $f_v$  at different stress

levels (ballast specimens)

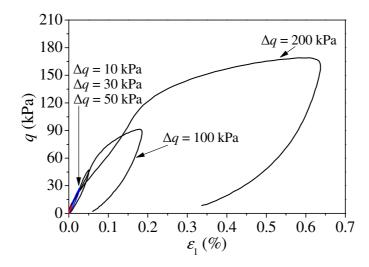


Fig. 11. Hysteresis loops at the first cycles of different stress levels for ballast

specimen at  $f_v = 20\%$ :  $\Delta q = 10$  kPa (N = 1),  $\Delta q = 30$  kPa (N = 101),  $\Delta q = 50$  kPa (N =

201),  $\Delta q = 100$  kPa (N = 701) and  $\Delta q = 200$  kPa (N = 1401)

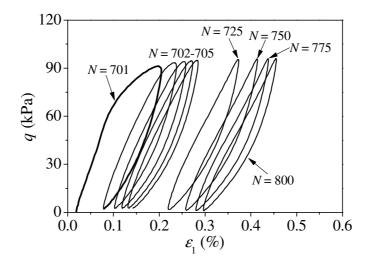


Fig. 12. Hysteresis loops during 100 cycles (N = 701 to 800) under  $\Delta q = 100$  kPa for

ballast specimen at  $f_v = 20\%$ 

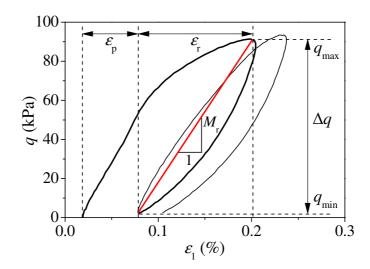


Fig. 13. Determination of  $M_r$ 

Note: The two hysteresis loops shown are the testing results of ballast specimen at  $f_v$  =

20% under  $\Delta q = 100$  kPa at cycle numbers of N = 701 and 702.

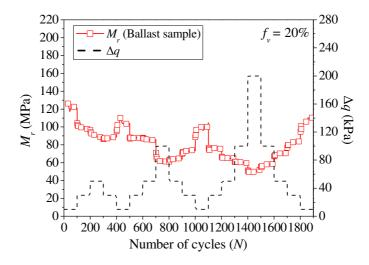


Fig. 14. Evolution of  $M_r$  with number of cycles at different stress levels for ballast

specimen at  $f_v = 20\%$ 

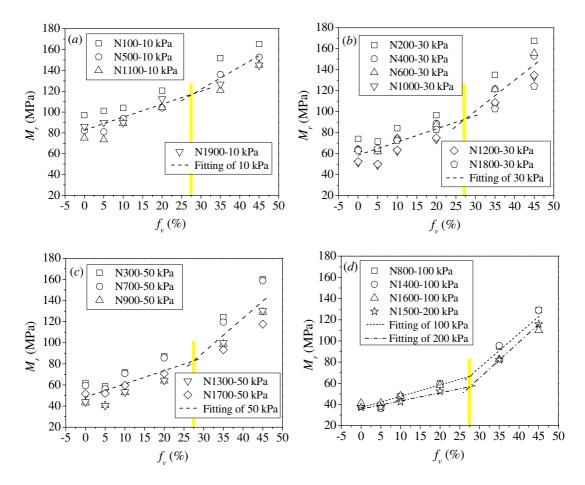


Fig. 15. Evolutions of  $M_r$  at end stage with  $f_v$  for ballast specimens at: (a)  $\Delta q = 10$  kPa;

(b)  $\Delta q = 30$  kPa; (c)  $\Delta q = 50$  kPa; (d)  $\Delta q = 100$  kPa and 200 kPa

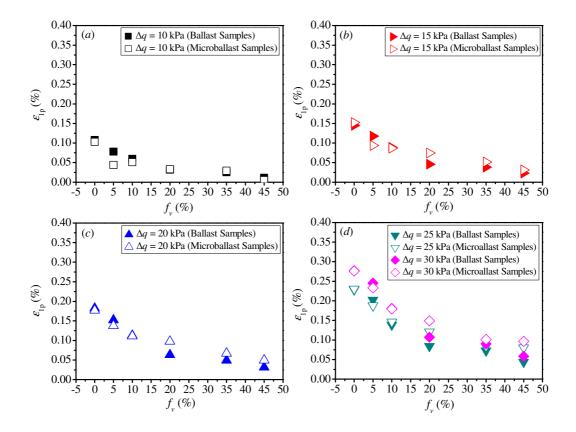


Fig. 16. Variations of estimated end-stage permanent strains with  $f_v$  for ballast and microballast specimens at: (a)  $\Delta q = 10$  kPa; (b)  $\Delta q = 15$  kPa; (c)  $\Delta q = 20$  kPa; (d)  $\Delta q$ 

= 25 kPa and 30 kPa

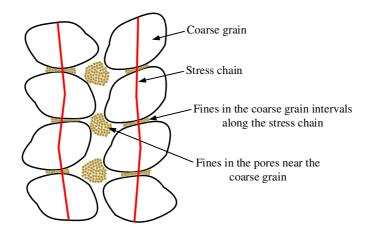


Fig. 17. Schematic illustration of the distribution of fines soils in case of grain-grain

contact structure

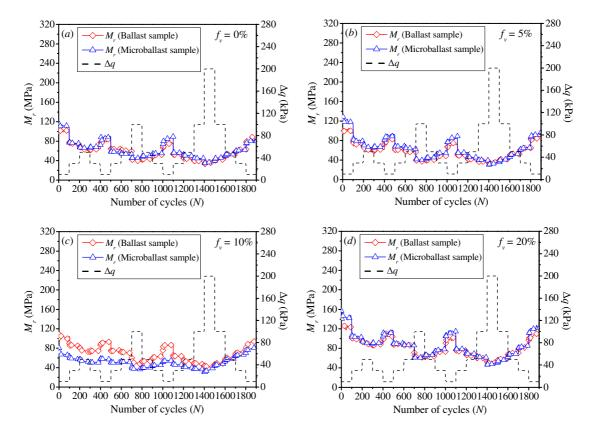


Fig. 18. Comparison of  $M_r$  value between ballast specimens and microballast

specimens in case of fine-fine contact structure for: (a)  $f_v = 0\%$ ; (b)  $f_v = 5\%$ ; (c)  $f_v =$ 

10%; (d)  $f_v = 20\%$ 

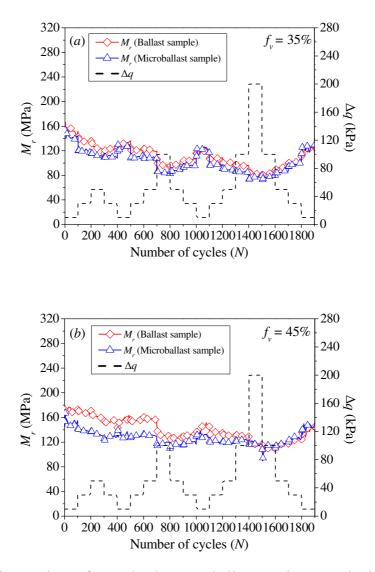


Fig. 19. Comparison of  $M_r$  value between ballast specimens and microballast specimens in case of grain-grain contact structure for (a)  $f_v = 35\%$  and (b)  $f_v = 45\%$ 

0.001 - 0.01 (20% of the particles)

0.0003 - 0.01 (80% of the particles)

0.0009 - 0.25 0.0009 - 0.50 0.063 - 0.50 0.16 - 0.63 0.25 - 1 0.32 - 2 0.32 - 2